The 2015 World Congress on
Advances in Structural Engineering and Mechanics (ASEM15)
Incheon, Korea, August 25-29, 2015

Behaviour of demountable CFST column-column connections

*Dongxu Li[1)], Brian Uy[2)] and Vipulkumar Ishvarbhai Patel[3)]

[1), 2), 3)] *Centre for Infrastructure Engineering and Safety, The University of New South Wales, Sydney, NSW 2052, Australia*
[1)] dongxu.li@student.unsw.edu.au
[2)] b.uy@unsw.edu.au
[3)] v.patel@unsw.edu.au

ABSTRACT

The amount of construction materials consumed by construction industry is increasing annually and many of these raw materials will run out by 2030. Moreover, the production and transport of building materials contributes significantly to greenhouse gas (GHG) emissions. Methods for lowering the negative influence on the environment can be achieved by reusing and recycling construction materials. Compared with other construction materials, structural steel can be reused multiple times with no loss of material properties and the actual reuse of structural steel only accounts for 10-15%, which means significant opportunities to grow market for the reuse of structural steel. However, one of the major limitations of the reuse of structural steel is the ability to render the structures demountable. This has created an urgent requirement to design innovative connections to allow the structures to be made demountable and subsequently make construction materials (mainly structural steel) reusable and recyclable.

Due to the wide application of steel-concrete composite structures, especially concrete-filled steel tubular (CFST) columns in industry, this research aimed at designing an innovative column-column and column-baseplate connections, which allow structures to be made demountable by utilising the demountable blind bolts and pre-welded sleeve plates. The approach and methodology to this research include design, experimental and analytical. The design of CFST column-column connections are based on the design codes, whilst for the experimental part, CFST column-column connections will be tested under axial compression and tension. The analytical phase involves developing finite element (FE) models using ABAQUS to assess the stiffness, strength and ductility for both connection types. In addition, the effects of various parameters on the behaviour of these CFST connections will be investigated based on the developed finite element models. These parameters include depth-to-thickness (D/t) ratio, concrete compressive strengths (f_c'), steel yield strengths (f_{sy}) and specimen length (L).

[1)] PhD scholar
[2)] Professor
[3)] Research associate

1. INTRODUCTION

Many kinds of raw materials will run out by 2030 (Gorgolewski, 2006) due to the increasing amount of construction materials consumed by the construction industry annually (Busby, 2002). Moreover, most of the greenhouse gas (GHG) emissions are attributed by the production and transport of the construction materials. To lower these negative influences on the environment, measures like reducing and reusing construction materials can be carried out. Furthermore, Winters-Downey (2010) pointed out that structural steel can be reused multiple times without the loss of material properties, compared with other construction materials. However, the ability of connections to be made demountable limits the reuse of the structural steel.

In addition, composite steel-concrete construction is one of the predominant structural forms for structural steel (Uy, 2014) and has been gaining attraction to designers due to its significant structural and economic benefits (Anderson and Najafi, 1994). In particular, the CFST columns have been extensively applied in the construction of building structures, bridges and other industrial structures.

Therefore, this research aims to design innovative column connections for steel-concrete composite structures. This innovative design will utilise blind bolted connections and subsequently enhancing the assembly and disassembly process, through which, not only the reduction as well as the reuse of structural steel can be promoted, but also safety and low cost in design are promoted. Furthermore, this research also aims to develop finite element (FE) models to carry out parametric studies to investigate the effects of various parameters on the behaviour of the demountable CFST column connections under axial compression and tension.

2. CFST COLUMN-COLUMN CONNECTION DESIGN AND CONSIDERATION

2.1. Design details

In this study, an innovative CFST column-column connection has been designed. As illustrated in Fig. 1, the top column will have a pre-welded sleeve plate extending past the base of the top columns. Demountable blind bolts are then to be connected through the sleeve plate and through the bottom columns. After removing the service load, which is about 40% of the ultimate compression load, the blind bolts can be removed as the head would be situated on the exterior of the tube and allows for ease of dismantling. Moreover, there is a base-plate pre-welded at the base of the top steel column, and the reinforcing bars located inside the top columns are welded to the base-plate. This design makes the infilled concrete and reinforcing bars discontinuous at the connection area, which can ensure the structures to be easily dismantled in the future.

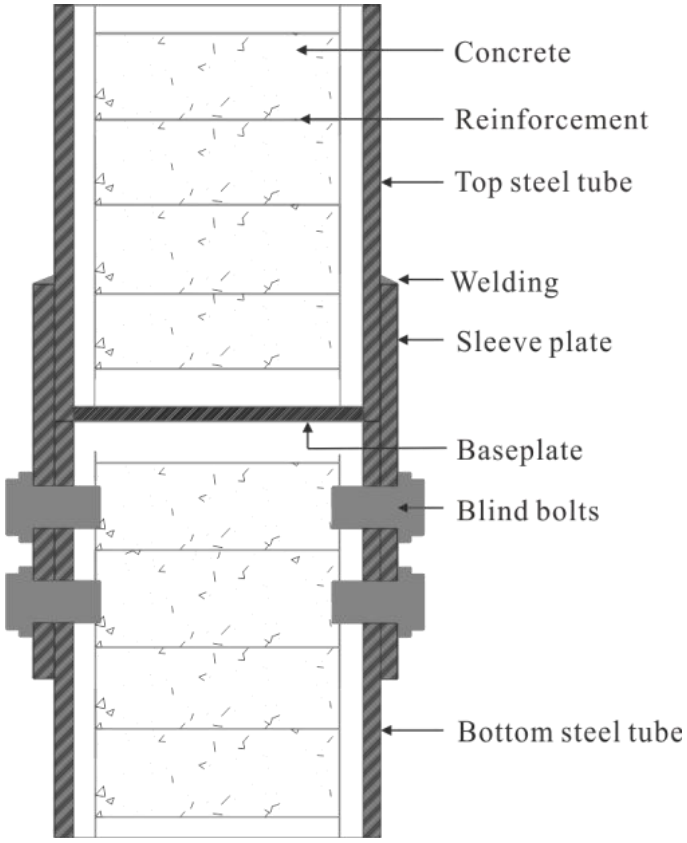

Fig. 1 CFST column-column splice connection

2.2. Design considerations

2.2.1. Design of CFST column-column connections under axial compression

CFST column-column connections are mainly designed for resisting axial compression load from typical loading regimes. The design in this study is in compliance with the AS 3600 (2009) and AS 4100 (1998). The compression capacity is assumed to be the summation of the compression capacity of steel tube and infilled concrete, although this value is smaller than the actual compression capacity of the connection due to the ignorance of the concrete confinement effect.

2.2.2. Design of CFST column-column connections under axial tension

As suggested by Eurocode 1 (1991), structures have to be designed sufficiently robust to sustain a limited extent of damage or failure without collapse. In the case of framed buildings, columns should be capable of resisting an accidental design tensile force equal to the largest design compression force applied to the column from any one story. According to AS 1170 (2002), tension capacity of the CFST column-column connection under accidental condition can be calculated as follows:

$$T_c = \eta \times N_c \tag{1}$$

where N_c is the compression capacity of the columns and η is the reduction factor, which is given by.

$$\eta = \frac{N_1}{N_o} \tag{2}$$

where N_0 stands for the compression load applied on column under normal condition, which is calculated by the equation given in AS 1170:

$$N_o = 1.2G + 1.5Q \tag{3}$$

where G represents the dead load in kPa. The dead load is assumed just the self-weight of slab and it can be calculated using the following formula:

$$G = \rho_{con} \times D_{slab} \tag{4}$$

where ρ_{con} depicts the unit weight of concrete, which is taken as 24 kN/m^3 from Table A1 in AS/NZS 1170; D_{slab} is the depth of slab, which is conservatively assumed as 0.15 m. In Equation (3), Q is taken as 3.0 kPa based on AS/NZS 1170.

In Eq. (2), N_1 is the compression load applied on column after earthquake, the load is determined using the equation given by AS/NZS 1170:

$$N_1 = G + \psi_e Q \tag{5}$$

where ψ_e is the reduction factor for live load after earthquake, taken as 0.3 based on AS/NZS 1170. Thus, regardless of the number of building stories or floor area contributed to the column, this reduction factor (η) is calculated as 51%.

In Eq. (2), N_1 can also be the compression load applied on column after fire, the load is determined using the equation given by AS/NZS 1170:

$$N_1 = G + \psi_l Q \tag{6}$$

where ψ_l is the reduction factor for live load after fire, taken as 0.4 based on AS/NZS 1170. Therefore, this factor (η) is calculated as 54%.

In this study, a reduction factor of 50% is to be used for all extreme conditions. This means a CFST column-column connection under extreme conditions should be capable of providing a tensile capacity equal to half of the compression capacity of the column-column connection.

2.2.3. Design for blind bolts arrangement

In this study, three types of CFST column-column connections are proposed with various cross-section sizes, 250×250 mm, 200×200 mm and 150×150 mm. For the column cross-section is 250×250 mm, the following design details for blind bolts and sleeve plate dimension are presented, which are based on the joint publication “Joints

in Steel Construction Simple Connections" by Steel Construction Institute (SCI) and British Constructional Steelwork Association (BCSA).

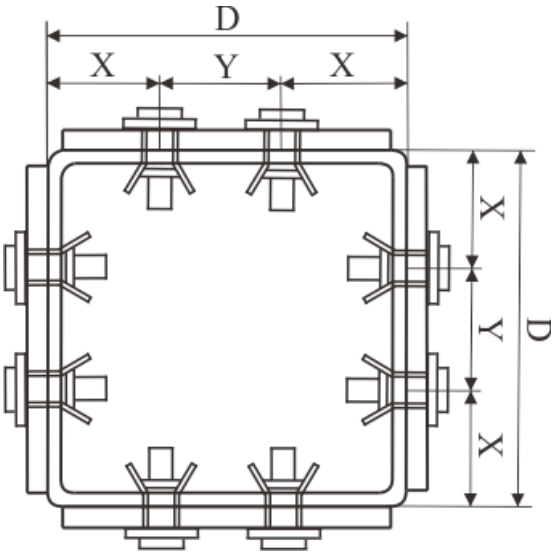

Fig. 2 Blind bolts arrangement for CFST connections

As illustrated in Fig. 2, centre-to-centre distance between two blind bolts (Y) is required not to be less than 70 mm, and bolt centre-to-edge distances (X) should be greater than 25 mm. Moreover, when putting blind bolts at adjacent surfaces, bolt centre-to-edge distance should be revised with Eq. (7), which can be calculated as:

$$E_1 = 90 - t_p \tag{7}$$

where t_p is the thickness of the sleeve plates, which has to be greater than 8 mm, to maximise the shear capacity of the blind bolts. In this study, to achieve better shear performance and higher connection stiffness, a conservative value of 10 mm was utilised. For the CFST cross-section size of 200×200 mm, the plan view of the bolt arrangement is identical with Fig. 2. However, the bolts in adjacent surface are staggered arranged with a vertical spacing of 35 mm.

3. FINITE ELEMENT ANALYSIS

As experimental studies on CFST column-column connections are expensive and time-consuming, it is necessary to conduct extensive numerical simulation for this connection before the commencement of the experimental work. In this study, the FEM program ABAQUS was used to develop an accurate FEM model for predicting the behaviour of demountable CFST column-column connections under axial compression. For the purposes of accurate FE analysis, element type, element mesh, boundary

condition, steel tube–concrete interface, material properties for steel tube and confined concrete, initial imperfections and residual stresses must all be considered.

3.1. General

Steel tubes, confined concrete, blind bolts, welding are modelled with eight-node brick elements with three translation degrees of freedom at each node (C3D8R), whilst the reinforcing bars are modelled with truss element (T3D2).

A study was carried out to establish a rational mesh size which provides consistent results with less computational time. Based on the study results, the rational mesh size for steel tubes and in-filled concrete is *B*/15 and *D*/3 for blind bolts. In addition, the reinforcing steel is modelled with truss element, and the rational mesh size is determined to be *L*/10.

Surface-to-surface contact is used to model the steel tube-concrete and steel tube-sleeve plate interfaces. A coefficient of friction between the steel tube and concrete is taken as 0.6, as suggested by Aslani et al. (2015). Compared to the interface between steel tube and concrete, interface of steel tube-sleeve plate has less friction, in this study, a coefficient of friction is taken as 0.3.

Fixed boundary conditions were applied to ties the end section surface to the reference point located at the centre of the end section. The clamped condition was used in this study, which fix all degrees of freedom except for the displacement at the loaded end. In addition, the specimen in this study is loaded under displacement control, which can facilitate the capture of descending branch of the axial load-strain curve.

3.2. Material properties for steel

Steel material properties specified in ABAQUS included the elastic and plastic behaviours. For the elastic behaviour, Young's modulus of steel (E_s) and Poisson's ratio (ν_s) are taken as 200,000 MPa and 0.3, respectively. In terms of the plastic behaviour, Tao et al. (2013) suggested that the rectangular CFST columns seldom demonstrates strain-hardening behaviour, due to the easier local buckling of the rectangular steel tube and less effective confinement provided to the concrete. For this reason, an elastic-perfectly plastic model of steel generates a better prediction of the descending branch of the load-strain curve than other models incorporating strain hardening. Thus, in this study, the elastic-perfectly plastic model (Fig. 3) is used to simulate the steel material (e.g. steel tube, sleeve plate and reinforcing bars) in rectangular CFST columns.

3.3. Material model for confined concrete

For a CFST column under axial compression, the infilled concrete expands laterally and is confined by the steel tube. This confinement is passive in nature and can increase the strength and ductility of the concrete. Furthermore, the confinement effect depends on the diameter-to-thickness ratio of the steel tube and material properties. In this FE analysis, the damage plasticity model defined in ABAQUS is used.

Damage plasticity model allows uniaxial compression stress-strain curve, tensile fracture energy and other parameters to be input. In this study, two confined concrete models are utilised to investigate the behaviour of CFST column connections.

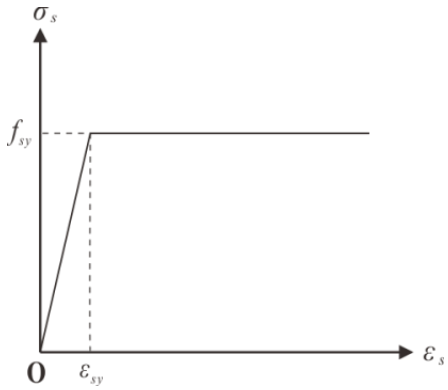

Fig. 3 Stress-stain relationship for structural steel

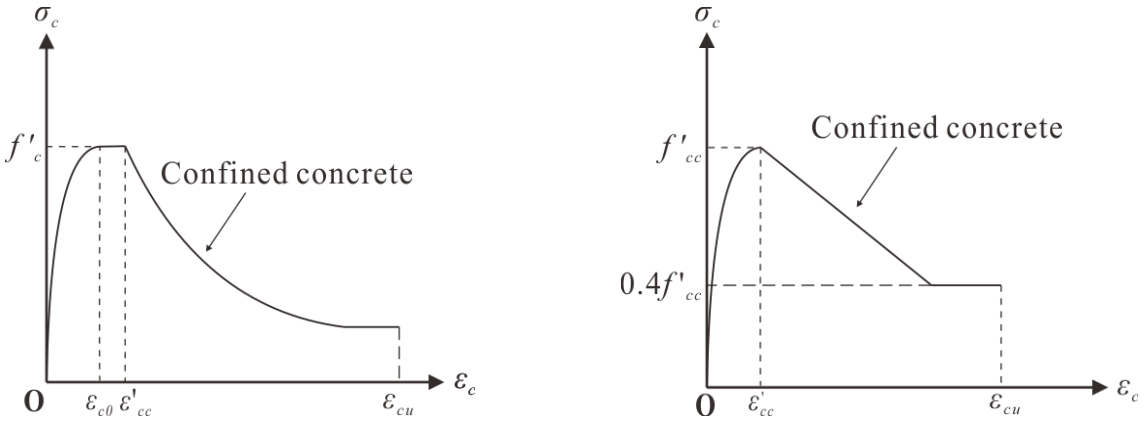

(a) Stress-stain relationship for confined concrete proposed by Tao et al. (2013)

(b) Stress-stain relationship for confined concrete given by Aslani et al. (2015)

Fig. 4 Two confined concrete models for finite element analysis

Fig. 4 (a) depicts the confined concrete model proposed by Tao et al. (2013). This type of confined concrete model is used for specimens with high *D*/*t* ratio. In the initial stage, there is little interaction between steel tube and confined concrete. Therefore, the ascending branch of the stress-strain curve of unconfined concrete is appropriate to be used until peak strength (f'_c) is reached. The following equations are used to describe this curve:

$$\frac{\sigma_c}{f_c^{'}} = \frac{AX + BX^2}{1+(A-2)X+(B+1)X^2} \qquad 0 < \varepsilon \le \varepsilon_{c0} \tag{8}$$

$$X = \frac{\varepsilon}{\varepsilon_{c0}} \tag{9}$$

$$A = \frac{E_c \varepsilon_{c0}}{f_c^{'}} \tag{10}$$

$$B = \frac{(A-1)^2}{0.55} - 1 \tag{11}$$

$$\varepsilon_{c0} = 0.00076 + \sqrt{(0.626 f_c^{'} - 4.33)\times 10^{-7}} \tag{12}$$

After that, a plateau part is incorporated to simulate the increased strain from confinement effects. Eqs. (13) to (15) are used.

$$\frac{\varepsilon_{cc}}{\varepsilon_{c0}} = e^k \tag{13}$$

$$k = (2.9224 - 0.00367 f_c^{'})(\frac{f_B}{f_c^{'}})^{0.3124+0.002 f^{'}_c} \tag{14}$$

$$f_B = \frac{0.25(1+0.027 f_y) e^{\frac{-0.02\sqrt{B^2+D^2}}{t}}}{1+1.6e^{-10}(f_c^{'})^{4.8}} \tag{15}$$

In the descending branch, a softening portion with increased ductility due to confinement is considered. Eqs. (16) to (20) are used to describe this behaviour:

$$\sigma_c = f_r + (f_c^{'} - f_r)\exp[-(\frac{\varepsilon - \varepsilon_{cc}}{\alpha})^{\beta}] \quad \varepsilon \geq \varepsilon_{cc} \tag{16}$$

$$f_r = 0.1 f_c^{'} \tag{17}$$

$$\alpha = 0.005 + 0.0075\xi_c \tag{18}$$

$$\beta = 0.92 \tag{19}$$

$$\xi_c = \frac{A_s f_y}{A_c f_c^{'}} \tag{20}$$

As suggested by ACI (2008), the tensile behaviour of the confined concrete is assumed to be linear until the tensile strength is reached, which is taken as $0.56(f_c')^{0.5}$. Beyond this failure stress, the tensile response is represented by fracture energy (GF). According to FIP (1993), fracture energy can be calculated through the following equation:

$$G_F = (0.0469 d^2{}_{\max} - 0.5 d_{\max} + 26)(\frac{f_c^{'}}{10})^{0.7} \tag{21}$$

Other parameters required to be determined include elastic modulus (E_c), Poisson's ratio (ν_c), dilation angle (Ψ), flow potential eccentricity (e), the ratio of initial

equibiaxial compressive yield stress to initial uniaxial compressive yield stress (f_{b0}/f'_c), shape factor of yield surface (K_c) and viscosity parameter. As suggested by ACI (2008), Poisson's ratio is adopted as 0.2 and the elastic modulus of concrete is determined as $E_c = 3320\sqrt{f_c^{'}} + 6900$, where $f_c^{'}$ is in MPa.

For Ψ, f_{b0}/f_c' and K_c, the values used in the FE analysis can be calculated as follows:

$$\psi = 40^{\circ} \tag{22}$$

$$\frac{f_{b0}}{f_c^{'}} = 1.5(f_c^{'})^{-0.075} \tag{23}$$

$$K_c = \frac{5.5}{5 + 2(f_c^{'})^{0.075}} \tag{24}$$

Fig. 4(b) presents the confined concrete model proposed by Aslani et al. (2015). This concrete model is used for specimens with low D/t ratio. The stress-strain curve of the concrete is calculated as Eqs. (25) to (35):

$$\sigma_c = f_{cc}^{'}\left[\frac{n(\frac{\varepsilon_c}{\varepsilon_{cc}^{'}})}{n-1+(\frac{\varepsilon_c}{\varepsilon_{cc}^{'}})^n}\right] \quad 0 < \varepsilon_c \le \varepsilon_{cc}^{'} \tag{25}$$

$$f_{cc}^{'} = f_c^{'}(1.81 - 0.02 \times \frac{D}{t}) \tag{26}$$

$$\varepsilon_{cc}^{'} = \varepsilon_c^{'}[1 + 5(\frac{f_{cc}^{'}}{f_c^{'}} - 1)] \tag{27}$$

$$\varepsilon_c^{'} = \begin{Bmatrix} 0.002 & f_{cc}^{'} < 28 \\ 0.002 + (f_{cc}^{'} - 28)/54000 & 28 < f_{cc}^{'} \le 82 \\ 0.003 & f_{cc}^{'} > 82 \end{Bmatrix} \tag{28}$$

$$n = [1.02 - 1.17\frac{E_{\sec}}{E_c}]^{-1.05} \tag{29}$$

$$E_{\sec} = \frac{f_{cc}^{'}}{\varepsilon_{cc}^{'}} \tag{30}$$

$$E_c = 3320\sqrt{f_c^{'}} + 6900 \tag{31}$$

$$\sigma_c = f_{cc}^{'} - \beta \frac{f_{cc}^{'}}{\varepsilon_{cc}^{'}}(\varepsilon_c - \varepsilon_{cc}^{'}) \geq 0.4 f_{cc}^{'} \quad \varepsilon_{cc}^{'} < \varepsilon_c \leq \varepsilon_{cu} \tag{32}$$

$$\sigma_c = 0.4 f_{cc}^{'} \qquad \varepsilon_c > \varepsilon_{cu} \tag{33}$$

$$\beta = \begin{cases} (0.048 f_c^{'} - 2.14) - (0.098 f_c^{'} - 4.57)(\frac{f_l}{f_c^{'}})^{1/3} & f_y \leq 550 \,\&\, f_c^{'} > 75 \\ 0.06 & f_y \leq 550 \,\&\, f_c^{'} \leq 75 \\ 0.07 & f_y > 550 \,\&\, f_c^{'} \leq 75 \\ 0.1 & f_y > 550 \,\&\, f_c^{'} > 75 \end{cases} \tag{34}$$

$$\frac{\varepsilon_{cu}}{\varepsilon_c^{'}} = \begin{cases} 2.0 + (70.0 - 0.6 f_c^{'}) \sqrt{\frac{f_l}{f_c^{'} f_c^{'}}} & f_c^{'} \leq 50 \\ 2.0 + (49.0 - 0.2 f_c^{'}) \sqrt{\frac{f_l}{f_c^{'}}} & f_c^{'} > 50 \end{cases} \tag{35}$$

3.4. Finite element model configurations

3.4.1. Configuration of blind bolt

To allow the CFST column-column connections to be demountable at the end of their service-life, blind bolts were used in this design research. Blind bolts include Flowdrill system, the Huck Blind bolt, the Ajax bolt, and the Lindapter Hollo-bolt. As studied by Hassan et al. (2014), the Lindapter Hollo-bolt performs better than other blind bolts. Thus, in this study, the Lindapter Hollo-bolts M20 of grade 8.8 are used.

For FE modelling, a simplified Hollo-bolt model is introduced as shown in Fig. 5. As in this study, the blind bolts are mainly applied with shear force; the bolt nuts are not modelled. In addition, the Hollo-bolt is modelled as tightened, which means the legs of the sleeve are spread with an angle of 15°.

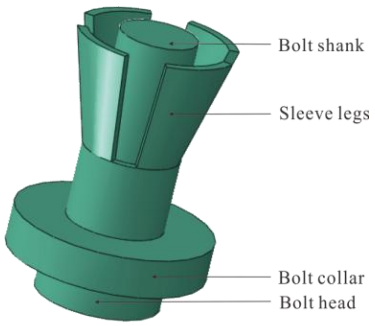

Fig. 5 Configuration of column-column connections.

3.4.2. Configuration of specimens

CFST column-column connections with various cross section sizes for the steel tube are determined, which is shown in Fig. 6.

All these designs utilise a sleeve plate with a thickness of 10mm. In particular, for the CFST column-column connections with 200 mm and 150 mm cross section size, blind bolts on adjacent surfaces are arranged in a staggered way, with a vertical spacing between two bolts 35 mm.

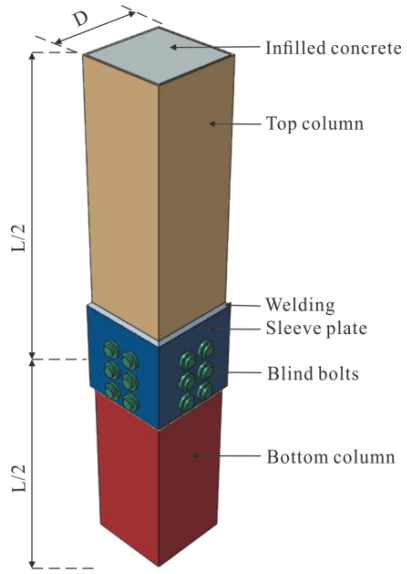

Fig. 6 Geometry of column-column connections.

4. PARAMETRIC STUDY

The FE models have been developed for this study. A parametric study in terms of the concrete compressive strength, steel yield strength, depth-to-thickness ratio, specimen length and connection position were performed to investigate the influence of these parameters on the structural behaviour of the CFST column-column connections under axial compression. Table 1 shows the different parameters and specimens considered for the FE analysis.

4.1. Effects of concrete strength (f'_c)

Fig. 7 presents the effects of concrete compressive strengths on the axial load-strain curves for CFST column-column connections under axial compression. The specimens 1-1-1 to 1-1-7, 2-1-1 to 2-1-7 and 3-1-1 to 3-1-7 in Table 1 are included in the analysis. It can be observed from Fig. 7 that the initial stiffness and ultimate axial strengths of CFST column-column connections increases with an increase in concrete compressive strength. The use of high strength concrete in CFST column-column connection reduces the ductility of this type of connection.

Table 1: Parameters considered for parametric studies

Specimen	$D \times t \times L$ (mm)	D/t	f'_c (MPa)	f_{sy} (MPa)	Position of connection	Concrete model	Group
1-1-1	250×9×1500	28	20	350	Mid-span	Aslani et al. (2015)	Group1
1-1-2	250×9×1500	28	25	350			
1-1-3	250×9×1500	28	32	350			
1-1-4	250×9×1500	28	40	350			
1-1-5	250×9×1500	28	50	350			
1-1-6	250×9×1500	28	80	350			
1-1-7	250×9×1500	28	100	350			
1-2-1	250×9×1500	28	32	250			
1-2-2	250×9×1500	28	32	300			
1-2-3	250×9×1500	28	32	450			
1-2-4	250×9×1500	28	32	500			
1-2-5	250×9×1500	28	32	690			
1-3-1	250×6×1500	42	32	350	Lower-Quarter Upper-Quarter	Tao et al. (2013)	
1-3-2	250×6×1500	42	32	350			
1-4-1	250×6×1500	42	32	350			
1-4-2	250×4×1500	63	32	350	Mid-span		
1-4-3	250×3×1500	83	32	350			
2-1-1	200×9×1200	22	20	350	Mid-span	Aslani et al. (2015)	Group 2
2-1-2	200×9×1200	22	25	350			
2-1-3	200×9×1200	22	32	350			
2-1-4	200×9×1200	22	40	350			
2-1-5	200×9×1200	22	50	350			
2-1-6	200×9×1200	22	80	350			
2-1-7	200×9×1200	22	100	350			
2-2-1	200×5×1200	40	32	250			
2-2-2	200×5×1200	40	32	300			
2-2-3	200×5×1200	40	32	350			
2-2-4	200×5×1200	40	32	450			
2-2-5	200×5×1200	40	32	500			
2-2-6	200×5×1200	40	32	690			
2-3-1	200×6×1200	33	32	350			
2-4-1	200×5×1500	40	32	350			
2-4-2	200×5×1200	40	32	350			
2-4-3	200×5×1000	40	32	350			
2-4-4	200×5×800	40	32	350			
2-4-5	200×5×600	40	32	350			
3-1-1	150×9×900	17	20	350	Mid-span	Aslani et al. (2015)	Group 3
3-1-2	150×9×900	17	25	350			
3-1-3	150×9×900	17	32	350			
3-1-4	150×9×900	17	38	350			
3-1-5	150×9×900	17	50	350			
3-1-6	150×9×900	17	80	350			
3-1-7	150×9×900	17	100	350			
3-2-1	150×9×900	17	32	250			
3-2-2	150×9×900	17	32	300			
3-2-3	150×9×900	17	32	450			
3-2-4	150×9×900	17	32	500			
3-2-5	150×9×900	17	32	690			
3-3-1	150×6×900	25	32	350			
3-3-2	150×5×900	30	32	350			

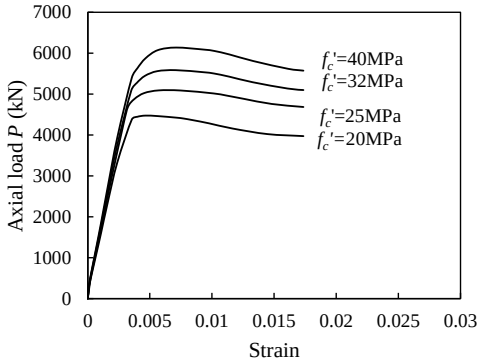

(a) Specimen 1-1-1 to 1-1-4

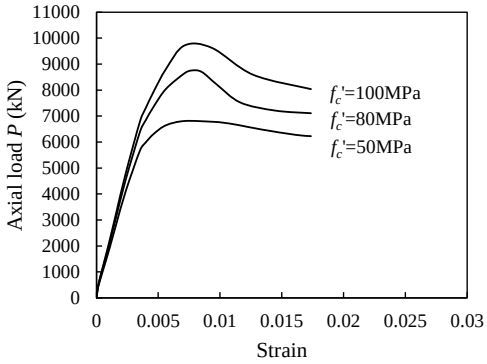

(b) Specimen 1-1-5 to 1-1-7

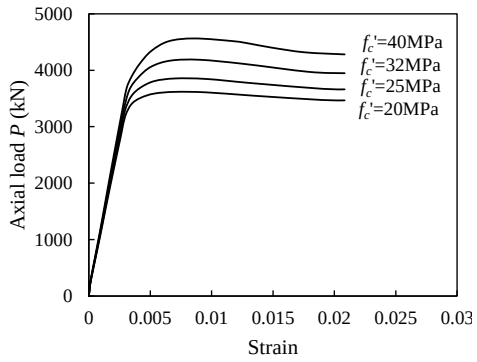

(c) Specimen 2-1-1 to 2-1-4

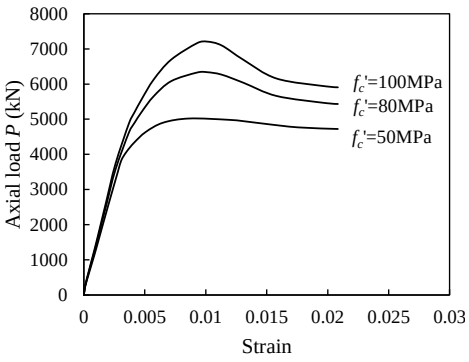

(d) Specimen 2-1-5 to 2-1-7

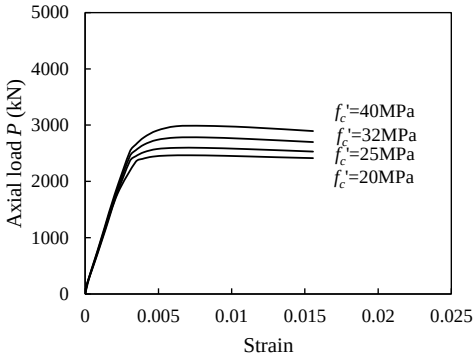

(e) Specimen 3-1-1 to 3-1-4

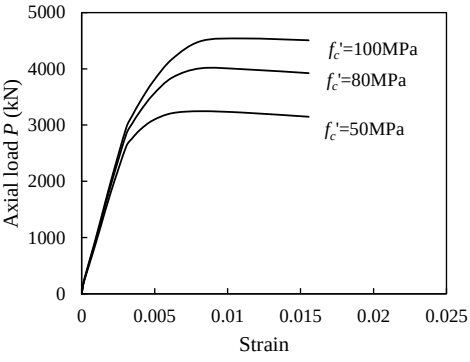

(f) Specimen 3-1-5 to 3-1-7

Fig. 7 Effects of concrete compression strengths on the axial load-strain curves for CFST column-column connections under axial compression.

4.2. Effects of steel strength (f_{sy})

The effects of steel yield strength on the axial load-strain curves for CFST column-column connections are shown in Fig. 8. The specimens 1-2-1 to 1-2-5, 2-2-1 to 2-2-5 and 3-2-1 to 3-2-5 are included in the analysis. It can be seen from the figure that the ultimate axial strength and ductility of CFST column-column connection increases with increasing the steel yield strength.

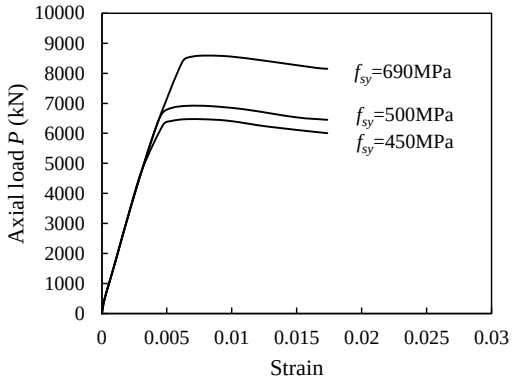

(a) Specimen 1-2-3 to 1-2-5

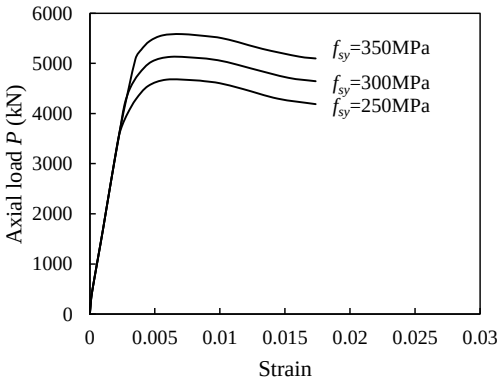

(b) Specimen 1-2-1 to 1-2-2 and 1-1-3

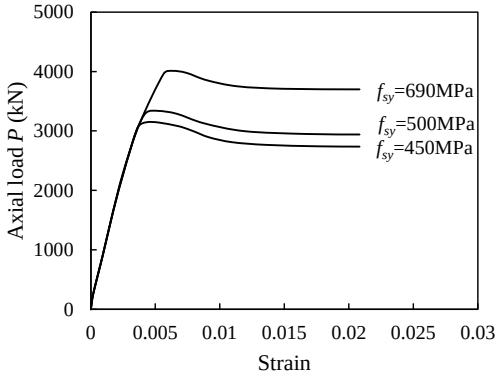

(c) Specimen 2-2-3 to 2-2-5

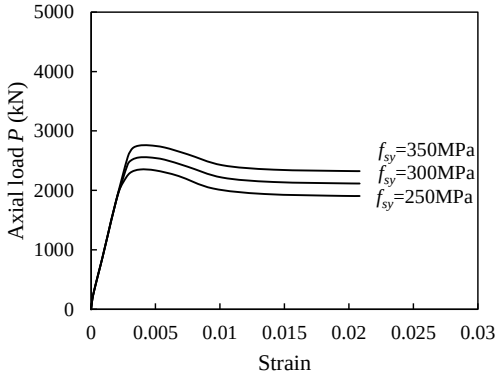

(d) Specimen 2-2-1 to 2-2-2 and 2-1-3

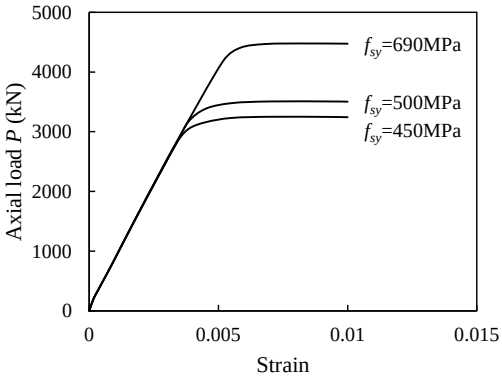

(e) Specimen 3-2-3 to 3-2-5

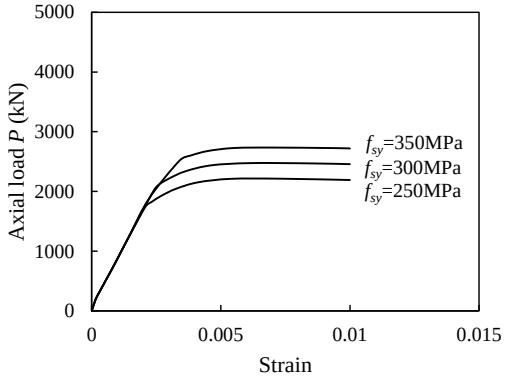

(f) Specimen 3-2-1 to 3-2-2 and 3-1-3

Fig. 8 Effects of steel yield strength on the axial load-strain curves for CFST column-column connections.

4.3. Effects of depth-to-thickness ratio (D/t)

Fig. 9 depicts the effects of depth-to-thickness ratio on the axial load-strain curves for Specimens 1-1-3, 1-4-1, 1-4-2 and 1-4-3. The material and geometric properties for these specimens are given in Table 1. It is noted from Fig. 9 that the initial stiffness and ultimate axial strength of CFST column-column connections decreases with an

increase in depth-to-thickness ratio of CFST column section. The ductility of the column-column connection improves with a decrease in the depth-to-thickness ratio.

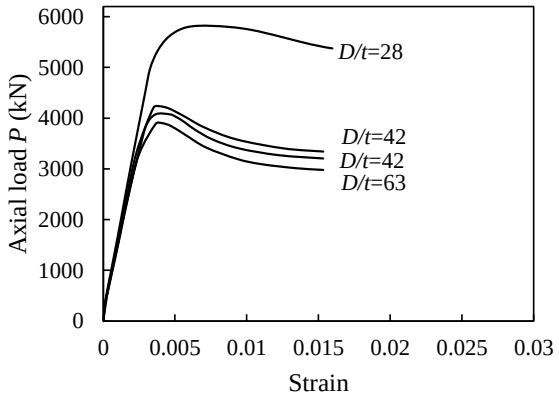

Fig. 9 Effects of depth-to-thickness ratio on the axial load-strain curves for CFST column-column connections.

4.4. Effects of specimen length (L)

Fig. 10 depicts the effects of specimen length on the axial load-strain curves for Specimens 2-2-3 and 2-4-1 to 2-4-4. It can be seen from Fig. 10 that the ductility, initial stiffness and ultimate strength of CFST column-column connections increase with a decrease in the specimen lengths. However, this effect is not significant when the specimen length ranges from 600 mm to 1000 mm.

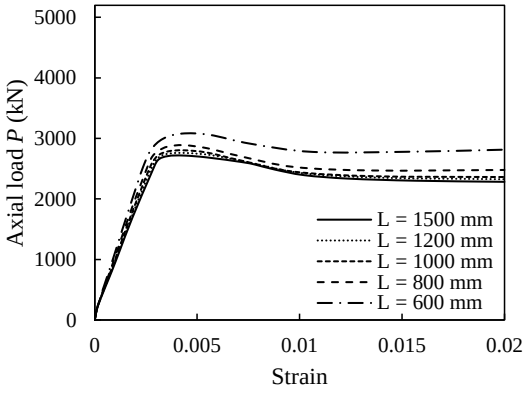

Fig. 10 Effects of specimen length on axial load-strain curves for CFST column-column connection.

4.5. Effects of connection position

Fig. 11 depicts the finite element model for different position of connection in CFST columns.

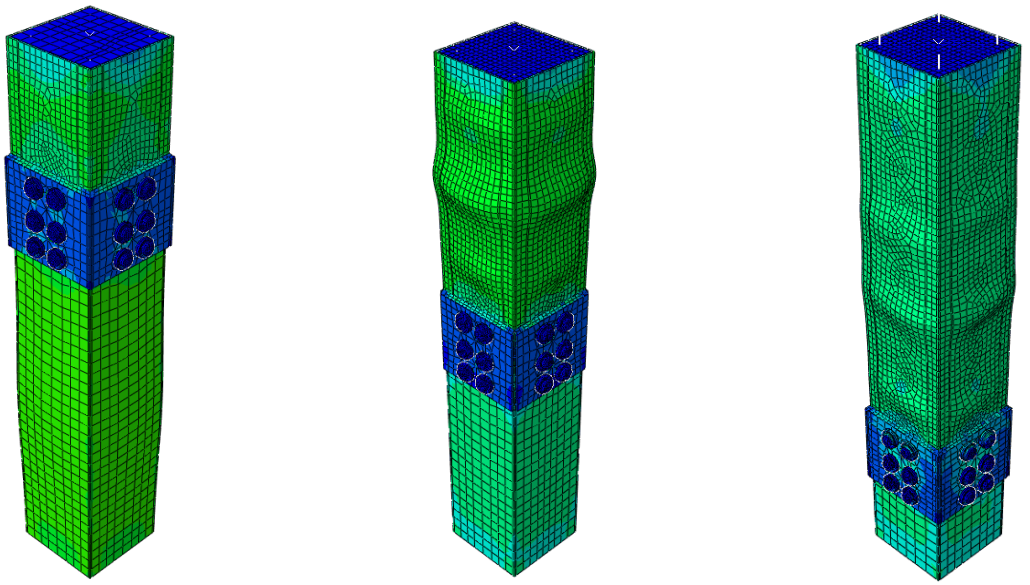

(a) Upper quarter (b) Mid-span (c) Lower quarter

Fig. 11 CFST column-column connection with various positions

The effects of connection positions on axial load-strain curves are demonstrated in Fig. 12. Specimens 1-3-1, 1-3-2 and 1-4-1 were used for analysis. It is shown that the ultimate axial strength of CFST with mid-span or upper quarter column-column connections is slightly higher than the lower quarter CFST column-column connection.

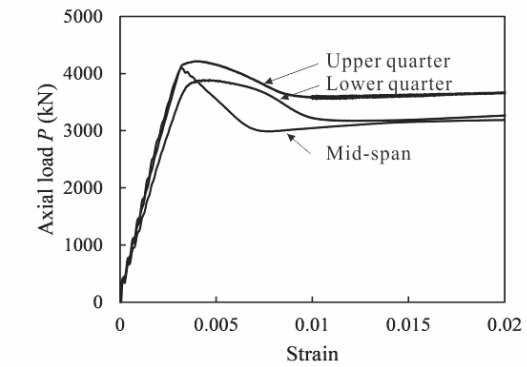

Fig. 12 Effects of connection position on axial load-strain curves for CFST column-column connections.

5. CONCLUSIONS

An innovative design for the CFST column-column connection has been proposed in this research study. Before conducting the expensive and time-consuming experimental work, an efficient computational FE model using ABAQUS is developed to simulate the axial load-strain behavior of the CFST column-column connections and to investigate the demountability of this connection. This FE model provides an efficient

means for structural analysis in order to develop design guidance for this application of composite structures.

A parametric study of different variables was performed to investigate the effects of pertinent parameters on the structural behaviour of the CFST column-column connections. From the parametric studies of this innovative connection, it can be concluded that:

(i) An increase in the concrete compressive strength causes an increase in the axial loading capacity and initial stiffness of this connection. But the ductility performance of this connection is negatively affected.

(ii) Increasing the steel yield strength will increase the axial compressive capacity and improve the ductility performance. However, the initial stiffness of this connection is not influenced significantly by the increase of steel strength.

(iii) The decrease of the depth-to-thickness ratio of the steel tube will increase the axial compressive capacity, initial stiffness and the ductility performance significantly, providing the concrete compressive strength and steel yield strength is fixed.

(iv) The ductility, initial stiffness and ultimate strength of CFST column-column connections increase with a decrease in the specimen lengths. However, for the specimens with a length less than 1000 mm, the effect of this parameter is not significant.

(v) The ultimate axial compressive strength of CFST upper quarter column-column connection is higher than the mid-span and lower quarter CFST column-column connections. Moreover, initial stiffness of the CFST upper quarter and mid-span column-column connections are higher than the CFST lower quarter column-column connection. In addition, CFST mid-span column-column connection has the worst performance in terms of the ductility.

ACKNOWLEDGMENTS

The research described in this paper is financially supported by the Australian Research Council (ARC) under its Discovery Scheme (Project No: DP140102134). The financial support is gratefully acknowledged.

REFERENCE

ACI-318. Building code requirements for reinforced concrete. Detroit, MI: ACI; 2008.

Anderson, D. and Najafi, A. A. 1994, “Performance of Composite Connections: Major Axis End Plate Joints”, *Journal of Constructional Steel Research*, vol. **31**, pp. 31-57.

Aslani, F., Uy, B., Tao, Z. and Mashiri, F. 2015, “Behaviour and design of composite columns incorporating compact high-strength steel plates”, *Journal of constructional Steel Research*, vol. **107**, pp. 94-110.

British Standards Institution. Eurocode 1: Actions on structures, Part 1.7 Accidental actions, DDENV 1991-1-7. *European Committee for Standardisation (CEN)*; 1991.

Busby, P. 2002, “Building Kyoto”. *Canadian Architect*, **47**(7): pp. 18-19.

FIP. CEB-FIP Model Code 1990. *Thomas Telford Ltd*., London, 1993.

Gorgolewski, M. 2006, “The implications of reuse and recycling for the design of steel buildings”, *Canadian Journal of Civil Engineering*, **33**: 489–496.

Standards Australia, Australian Standard AS 1170-2002. Structural design actions. *Standards Australia International Ltd*.; 2002.

Standards Australia, Australian Standard AS 3600-2009. Concrete structure. *Standards Australia International Ltd.*; 2009.

Standards Australia, Australian Standard AS 4100-1998. Steel structure. Standards Australia International Ltd.; 1998.

Tao, Z., Wang, Z. B. and Yu, Q. 2013, “Finite element modelling of concrete-filled steel stub columns under axial compression”, *Journal of Constructional Steel Research*, vol. **89**, pp. 121-131.

Uy, B. 2014, “Innovative connections for the demountability and rehabilitation of steel”, *Space and composite structures*, Prague, Czech Republic.

Winters-Downey, E. 2010, “Reclaimed structural steel and LEED Credit MR-3 – Materials Reuse”, *Modern Steel Construction*, May.